AD-A141 022 COMPUTATION OF THE NONEQUILIBRIUM FLOW IN A GASDYNAMIC LASER(U) FOREIGN TECHNOLOGY DIV WRIGHT-PATTESSON AFB OH H H YEN ET AL. 25 APR 84 FTD-ID(RS)T-0311-84 1/1

UNCLASSIFIED F/G 20/5 NL

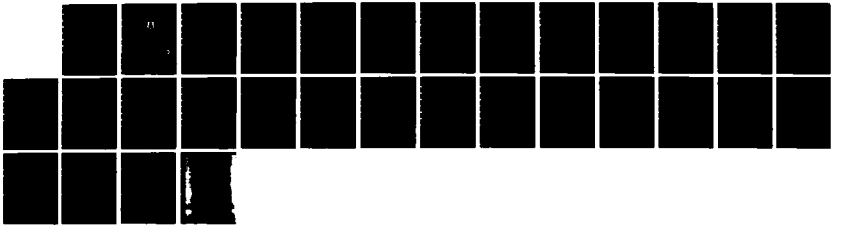

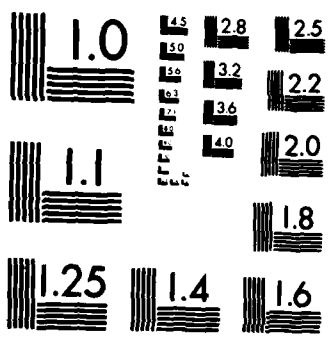

FTD-ID(RS)T-0311-84

FOREIGN TECHNOLOGY DIVISION

COMPUTATION OF THE NONEQUILIBRIUM FLOW IN A GASDYNAMIC LASER

by

Yen Hai-hsing, Chen Li-yin

EDITED TRANSLATION

FTD-ID(RS)T-0311-84 25 April 1984

MICROFICHE NR: FTD-84-C-000431

COMPUTATION OF THE NONEQUILIBRIUM FLOW IN A GASDYNAMIC LASER

By: Yen Hai-hsing, Chen Li-yin

English pages: 26

Source: Lixue Xuebao, Vol. 10, Nr. 4, 1978, pp. 274-287

Country of origin: China
Translated by: SCITRAN
F33657-81-D-0263
Requester: FTD/TQTD

PREPARED BY:

TRANSLATION DIVISION
FOREIGN TECHNOLOGY DIVISION
WP-AFB, OHIO.

GRAPHICS DISCLAIMER

All figures, graphics, tables, equations, etc. merged into this translation were extracted from the best quality copy available.

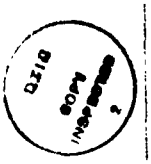

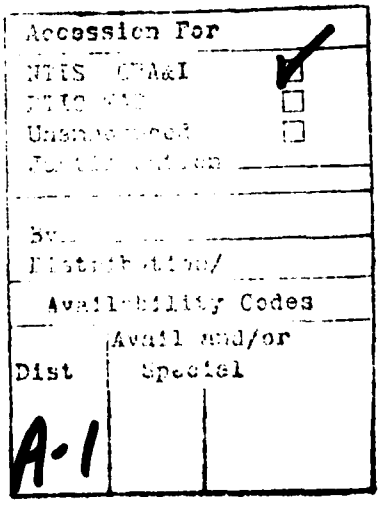

COMPUTATION OF THE NONEQUILIBRIUM FLOW IN A GASDYNAMIC LASER

Yen Hai-hsing, Chen Li-yin*
(Institute of Mechanics, Academia Sinica)

ABSTRACT

In this paper, we present a three-modes-four-temperatures vibrational relaxation model for the CO_2-N_2-H_2O laser system, and give a set of fairly rigorous relaxation equations. We have analyzed a series of problems related to computations of pseudo-one-dimensional non-equilibrium flows, and have carried out massive numerical computations using the data we obtained for the rate of relaxation. Our computed results, unlike those of other authors, agree fairly well with experimental results. The performance of the laser can be effectively improved by increasing the expansion area ratio. Appropriately decreasing the height of the throat also proves to be helpful. For combustion type gasdynamic lasers, there is an optimal value for the stagnation temperature, which lies between 1400 and 1600°K. Contrary to Anderson's conclusion, our computed results show that in a nozzle flow with a high stagnation temperature and a large area ratio, the optimal water content is still in the neighborhood of 1%. The performance of the unit quickly deteriorates with increasing water content. We have studied the effect of the various section of the shape-curve of the nozzle on the performance of the unit. We have also given a preliminary discussion of the effect of the relaxation model, equations and data on the computation, and have shown that the results of computation are very much affected by these factors.

*Comrade Sheng Chia-chu participated in writing part of the computer program.

I. Introduction

Gasdynamic lasers are a new type of high power laser that appeared near the end of the 60's. These lasers have received great attention in recent years, and have developed very rapidly [1]. Theoretical analyses have played an important role in every stage of the development of gasdynamic lasers. In particular, computations of pseudo-one-dimensional vibrational non-equilibrium flow have provided useful means for designing and improving gasdynamic lasers.

The computation of pseudo-one-dimensional non-equilibrium flow falls into two types. One is the steady-state method first adopted by , et al., [2]-[6]. In this approach, the pseudo-one-dimensional flow equations are solved simultaneously with the vibrational relaxation equations. The set of ordinary differential equations obtained are solved by means of the Runge-Kutta method. As there are singularities at the sonic points near the convergent-divergent nozzle, it is not possible to find a simple unified solution for the entire nozzle. To simplify the calculations, the subsonic section of the nozzle is usually assumed to be in equilibrium, and the equilibrium flow is calculated starting from the throat. To overcome the difficulty with the singularities, certain techniques of parameter adjustment are used to obtain convergent solutions for the set of equations.

The other type is the non-steady-state method adopted by Anderson [7]. In this approach, a distribution of initial values at time t=0 is first assumed for each of the unknown variables in the set of non-steady-state equations. Then, a difference scheme is used to find the values of the variables at time $t+\Delta t$ (the time step size Δt being required to meet certain stability conditions) from their values at time t. The process is repeated until, at a fairly large t, all the parameters converge to their steady-state values. These types of equations are hyperbolic for the entire nozzle. No singularity

exists at the throat region. The entire nozzle can thus be solved for as a whole. As a result, the nonequilibrium effects at the subsonic section of the nozzle are automatically included in the computation, and possible errors due to artificially introduced adjustments in the numerical calculations are avoided. The obvious advantage of this method has made it very popular in theoretical computations on gasdynamic lasers [8]-[13].

However, researchers abroad have either used simplified relaxation models in their computations, or employed erroneous relaxation equations. In addition, most of these computations have not included the latest relaxation data. Hence, certain deviations or contradictions exist between their computed results and the experimentally measured values [14],[10].

In this paper, we present a three-modes-four-temperature relaxation model, and give a set of fairly rigorous relaxation equations. The equations for computing nonequilibrium flows will be listed, some problems related to the numerical calculations will be discussed, and the main computed results will be given and compared with the theoretical and experimental results obtained by others. We will also give an analysis of certain related problems.

II. Relaxation model and relaxation equations

The rate of vibrational relaxation of the "catalyst" H_2O in the CO_2-N_2-H_2O laser system is very high, so that the various vibrational modes can always be regarded as being approximately in equilibrium with the average motion. Thus, the V-V exchange among the molecules of H_2O and those of CO_2 and N_2 is equivalent to the result of regarding H_2O as collision partners for CO_2 and N_2 molecules in their molecular relaxation process [15]. The vibrational energy level diagram and energy exchange processes for the laser system are given in Figure 1. The vibrational relaxation processes are:

V-T exchange

$$CO_2^*(\nu_2) + M \rightleftharpoons CO_2 + M + 667cm^{-1} \quad (1)$$

$$N_2^* + M \rightleftharpoons N_2 + M + 2331cm^{-1} \quad (2)$$

intermolecular V-V exchange

$$CO_2^*(\nu_3) + N_2 \rightleftharpoons CO_2 + N_2^* + 18cm^{-1} \quad (3)$$

$$CO_2^*(\nu_3) + M \rightleftharpoons CO_2^{**}(\nu_2) + M + 416cm^{-1} \quad (4)$$

intramolecular V-V exchange

$$CO_2^*(\nu_1) + M \rightleftharpoons CO_2^{**}(\nu_2) + M + 102cm^{-1} \quad (5)$$

In the above, * denotes a quantum of vibrational energy. The collision partner $M = CO_2, N_2, H_2O(C, N, H)$. The relaxation equations are

$$\frac{dE_1}{dt} = \left(\frac{dE_1}{dt}\right)_{\nu_1 \to 2\nu_2} + \left(\frac{dE_1}{dt}\right)_{\text{radiative}} \quad (6)$$

$$\frac{dE_2}{dt} = -\frac{2\theta_2}{\theta_1}\left(\frac{dE_1}{dt}\right)_{\nu_1 \to 2\nu_2} + \left(\frac{dE_2}{dt}\right)_{\nu_2 \to T} + \left(\frac{dE_2}{dt}\right)_{\nu_3 \to 2\nu_2} \quad (7)$$

$$\frac{dE_3}{dt} = -\frac{\theta_3}{3\theta_2}\left(\frac{dE_2}{dt}\right)_{\nu_3 \to 2\nu_2} + \left(\frac{dE_3}{dt}\right)_{\nu_3 \to \nu_N} + \left(\frac{dE_3}{dt}\right)_{\text{radiative}} \quad (8)$$

$$\frac{dE_N}{dt} = -\frac{\theta_N}{\theta_1}\left(\frac{dE_2}{dt}\right)_{\nu_1 \to \nu_N} + \left(\frac{dE_N}{dt}\right)_{\nu_N \to T} \quad (9)$$

In the above, E_1, E_2, E_3, E_N are, respectively the vibrational energy stored in the vibrational modes $CO_2(\nu_1)$, $CO_2(\nu_2)$, $CO_2(\nu_3)$ and N_2 of a unit mass (g) of the gas mixture: $E_i = \frac{g_i N_i k \theta_i}{e^{\theta_i/T_i} - 1}$ (10)

Here $N_1 = N_2 = N_3 = N_C$ and N_N are, respectively, the number of molecules of CO_2 and N_2 per gram of the gas mixture: g_i is the degree of degeneracy, which is 1 except for g_2 which is 2; T_i is the vibrational temperature; θ_i is the characteristic vibrational temperature; k is Boltzmann's constant.

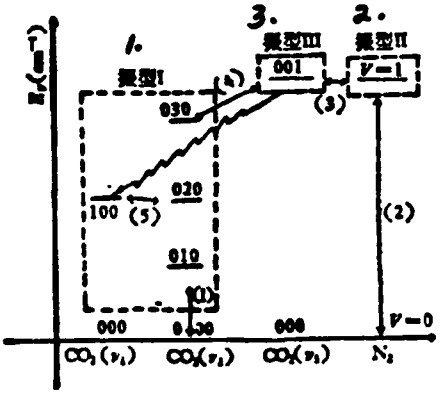

Figure 1. CO_2-N_2 vibrational energy level diagram
1--vibrational model I; 2--vibrational mode II; 3--vibrational mode III

It can be derived from the general vibrational relaxation equations [16] that

$$\left(\frac{dE_2}{ds}\right)_{v_2\to T} = \sum_M N_M^{(V)} K[C2(1\to 0); M] \times [E_2(T) - E_2] \tag{11}$$

276

$$\left(\frac{dE_2}{ds}\right)_{v_1\to v_2} = \sum_M N_M^{(V)} K[C3(1\to 0),\ C2(0\to 3); M] \times 3N_C k\theta_2 \times \left[\left(\frac{E_1}{N_C k\theta_1}\right)\left(\frac{E_2}{2N_C k\theta_2}+1\right)^3 - \left(\frac{E_1}{N_C k\theta_1}+1\right)\left(\frac{E_2}{2N_C k\theta_2}\right)^3 e^{(2\theta_2-\theta_1)/T}\right] \tag{12}$$

$$\left(\frac{dE_2}{ds}\right)_{v_1\to v_N} = N_M^{(V)} K[C3(1\to 0), N(0\to 1)] \times N_C k\theta_2 \times \left[e^{(\theta_N-\theta_2)/T}\left(\frac{E_2}{N_C k\theta_2}+1\right)\left(\frac{E_N}{N_N k\theta_N}\right) - \left(\frac{E_2}{N_C k\theta_2}\right)\left(\frac{E_N}{N_N k\theta_N}+1\right)\right] \tag{13}$$

$$\left(\frac{dE_N}{ds}\right)_{v_N\to T} = \sum_M N_M^{(V)} K[N(1\to 0); M] \times [E_N(T) - E_N] \tag{14}$$

$$\left(\frac{dE_1}{ds}\right)_{v_1\to v_2} = \sum_M N_M^{(V)} K[C1(1\to 0),\ C2(0\to 2); M] \times N_C k\theta_1 \times \left[\left(\frac{E_1}{N_C k\theta_1}+1\right)\left(\frac{E_2}{2N_C k\theta_2}\right)^2 e^{(2\theta_2-\theta_1)/T} - \left(\frac{E_1}{N_C k\theta_1}\right)\left(\frac{E_2}{2N_C k\theta_2}+1\right)^2\right] \tag{15}$$

In the above, the equilibrium vibrational energy $E_2(T)$ and $E_N(T)$ have, respectively, been obtained from equation (10) by substituting the vibrational temperature T_2 and T_N with the temperature T of the average motion. $N_M^{(V)}$ is the density of particles of the constituent M per unit volume (cm^3): $N_M^{(V)} = \rho N_M$ (16)

ρ is density (g/cm^3), and K is the coefficient of the rate of the vibrational relaxation process.

As Fermi resonance exists between the ν_1, ν_2 modes of CO_2, the process of $CO_2(\nu_1 \to 2\nu_2)$ is very rapid. In other words, the value of $K[C1(1\to 0),\ C2(0\to 2)$ is very large. If at a certain instant the vibrational energy of the ν_1 and ν_2 vibrational modes does not satisfy

$$\left(\frac{E_1}{N_C k\theta_1}+1\right)\left(\frac{E_2}{2N_C k\theta_2}\right)^2 e^{(2\theta_2-\theta_1)/T} - \left(\frac{E_1}{N_C k\theta_1}\right)\left(\frac{E_2}{2N_C k\theta_2}+1\right)^2 \approx 0 \tag{17}$$

then it can be seen from equation (15) that a large value of K will result in a high rate of change with time of E_1, $\frac{dE_1}{dt}$, and the ν_1 vibrational mode will equilibrate with the ν_2 mode in a very short

time. This means that as long as E_1 and E_2 do not satisfy equation (17), the rapid $CO_2(\nu_1 \rightarrow 2\nu_2)$ relaxation process will cause the left-hand side of equation (17) to go to zero in a negligible interval of time. Thus, we think equation (17) is a very good approximation. It can be easily derived from equation (17) that

$$\frac{\theta_1}{T_1} - \frac{2\theta_2}{T_2} = \frac{\theta_1 - 2\theta_2}{T} \tag{18}$$

This is the condition for equilibrium of the ν_1, ν_2 modes. It is worth noting that the condition $T_1 = T_2$ used by Anderson, et al., is valid only when one further assumes that $\theta_1 \approx 2\theta_2$ or $T_2 = T$. In all other cases, $T_2 > T_1 > T$.

Now we can combine the ν_1, ν_2 modes to form the vibrational mode I, with vibrational energy given by

$$E^I = E_1 + E_2 \tag{19}$$

We have from equations (6) and (7)

$$\frac{dE^I}{dt} = \underbrace{\left(\frac{dE_3}{dt}\right)}_{\text{radiative}} + \frac{\theta_1 - 2\theta_2}{\theta_1}\left(\frac{dE_1}{dt}\right)_{\nu_1 \rightarrow 2\nu_2} + \left(\frac{dE_2}{dt}\right)_{\nu_2 \rightarrow \nu_1} + \left(\frac{dE_2}{dt}\right)_{\nu_2 \rightarrow T} \tag{20}$$

Let us analyze the magnitude of each term. Although the terms enclosed in the right-most square brackets in equation (15) are very small, as K is fairly large, $\left(\frac{dE_1}{dt}\right)_{\nu_1 \rightarrow 2\nu_2}$ is not necessarily small. In fact, in the absence of a radiation field, we have

$$\frac{\left(\frac{dE_1}{dt}\right)_{\nu_1 \rightarrow 2\nu_2}}{\left(\frac{dE_2}{dt}\right)_{\nu_2 \rightarrow T} + \left(\frac{dE_2}{dt}\right)_{\nu_2 \rightarrow 2\nu_2}} \approx \frac{2e^{\theta_2/T_2}}{(e^{\theta_2/T_2} + 1)^2} \tag{21}$$

with values equal to 0.-0, 0.39 and 0.45, respectively, when T_2 is 350, 1000 and 1500°K. In other words, it is not appropriate to eliminate the term $\left(\frac{dE_1}{dt}\right)_{\nu_1 \rightarrow 2\nu_2}$ from equations (6) and (7). However, in equation (20), as $(\theta_1 - 2\theta_2)/\theta_1 = 0.0387$, the term $\frac{\theta_1 - 2\theta_2}{\theta_1}\left(\frac{dE_1}{dt}\right)_{\nu_1 \rightarrow 2\nu_2}$ is negligible compared to the other terms in this equation. A confession is due here in that part of the reason for wanting to eliminate this term lies in the lack of reliable data for $K[C1(1 \rightarrow 0), C2(0 \rightarrow 2)$; M]. Otherwise, one could use equation (15) directly in equations (6) and (7), and compute, without much difficulty, according to a four-vibrational modes-four-temperatures model.

We can use the equilibrium condition equation (18) to transform equation (20) into

$$\frac{dE_2}{dt} = \left[\frac{4N_C^2 k\theta_1 k\theta_2 e^{(\theta_1-2\theta_2)/T}(2N_C k\theta_2/E_2+1)}{E_2^2\{e^{(\theta_1-2\theta_2)/T}(2N_C k\theta_2/E_2+1)^2-1\}^2}+1\right]^{-1}$$
$$\times\left[\left(\frac{dE_1}{dt}\right)_{\text{radiative}}+\left(\frac{dE_2}{dt}\right)_{v_1-3v_2}+\left(\frac{dE_2}{dt}\right)_{v_2-T}\right. \qquad (22)$$
$$\left.-\frac{N_C k\theta_1(2N_C k\theta_2/E_2+1)^2 e^{(\theta_1-2\theta_2)/T}}{\{e^{(\theta_1-2\theta_2)/T}(2N_C k\theta_2/E_2+1)^2-1\}^2}\times\frac{\theta_1-2\theta_2}{T^2}\times\left(\frac{dT}{dt}\right)\right]$$

This equation, along with equations (8) and (9), make up the set of equations for the three-modes-four-temperatures relaxation model of this paper. The various terms in the above equations are given by equations (11)-(14).

The inaccuracy of the data for relaxation rate has a large effect on the outcome of nonequilibrium flow computations [17,13]. Most authors have based their computations on the data given in [15]. Many experimental results on relaxation were later published, and these contained additional data or modifications of previous data that have a rather great effect on particle number inversion. We have collected and processed experimental data of the relaxation rate coefficients for the processes given in equations (1)-(4), and have arrived at the following relation for K and temperature T:

$$\log_{10}\left(\frac{K}{G}\right) = A + BT^{-1/3} + CT^{-2/3} + DT^{-1}$$

The coefficients A, B, C and D have been given for each of the reactions. G is a combinatorial factor. For reactions (1)-(3), G = 1; for reaction (4), G = 4.

The computations made in this work are based on the above three-modes-four-temperatures model and the more rigorous set of relaxation equations, and make use of the relaxation data that we have collected and processed ourselves.

The relaxation model and equations of Anderson are still being used widely. A brief discussion of these is in order here. Anderson regards $CO_2(v_3)$ to be in equilibrium with the vibrational modes

of N_2, and considers their vibrational temperatures to be the same, thus forming mode II. This kind of assumption is not permissible in the presence of radiation fields. As the lasing process depends to a large degree on the relaxation rate of the transfer of the vibrational energy stored in N_2 to the $CO_2(\nu_3)$ vibrational mode, regarding the two vibrational modes as being in equilibrium is equivalent to considering the relaxation rate to be infinitely large. This is obviously not appropriate. Even in calculations involving small signal gains, errors will result. For the typical laser composition $X_C:X_N:X_H = 0.14:0.85:0.01$, the computed relaxation times are given in Table 1.

TABLE 1

$T(°K)$	300	500	1000	1500
$\tau p_{CO_2(\nu_3)\to 3\nu_2}(\mu s \cdot atm)$	3.02	2.04	0.405	0.096
$\tau p_{CO_2(\nu_3)\to N_2}(\mu s \cdot atm)$	0.078	0.174	0.480	0.630

278

It can be seen from the above table that at high temperatures, the relaxation rate of $CO_2(\nu_3)\to N_2$ is even slower than that of $CO_2(\nu_3\to 3\nu_2)$. Furthermore, the results of computation show that for a nozzle with $A/A^* \approx 30$, and h* = 0.3mm, $T_0 = 1500°K, p_0 = 30atm$ $X_C:X_N:X_H = 0.14:0.85:0.01$. T_N is higher than T_3 by up to 130°K inside the nozzle; and at the exit, T_N is also higher than T_3, by 40°K. This difference between T_N and T_3 is even more pronounced when A/A* is increased and h* is reduced.

Another problem lies in the fact that Anderson used the linearized relaxation equations for both modes I and II:

$$\frac{dE^{I}}{dt} = \frac{1}{\tau_{\nu_3\to T}}[E_1(T) + E_2(T) - E_1 - E_2] \tag{23}$$

$$\frac{dE^{II}}{dt} = \frac{1}{\tau^{II}}[E_3(T) + E_N(T) - E_3 - E_N] \tag{24}$$

Using equation (24) is equivalent to expanding the relaxation term for $CO_2(\nu_3\to 3\nu_2)$, i.e., equation (12), and taking only one linear term, omitting the others. This is only valid in the case where $T_2 = T$, which is not true in gas dynamic lasers. In equation (23), Anderson

has omitted the effect of the $CO_2(\nu_3 \rightarrow 3\nu_2)$ process on mode I, and has artificially introduced the term $[E_1(T) - E_1]/\tau_{\nu_3 \rightarrow T}$. The term

$$\frac{E_1(T) - E_1}{E_3(T) - E_3} \approx \frac{e^{\theta_2/T_2} + e^{\theta_2/T}}{(e^{\theta_2/T_2} + 1)(e^{\theta_2/T} + 1)}$$

is 0.075 when $T_2 \approx T=300°K$. It can be as large as 0.78 at 1000°K. Thus, a fairly large term has been introduced artificially. Some of Anderson's computed results agree better with experimental results. This may be due to the fact that the approximations in the relaxation model and relaxation equations have certain errors that cancel each other, and the fact that the not very accurate relaxation data have compensated the inadequacies of the model and the equations.

III. Equations

For the two-dimensional nozzle that is usually used in gas-dynamic lasers, if one assumes that the various parameters are constant across the flow, the problem reduces to that of a pseudo-one-dimensional flow. In addition, we assume the fluid to be an ideal fluid, and neglect any inhomogeneity in the flow (such as boundary layer, wake, shock waves, etc.) and heat transfer effects. Such approximations work better for a single nozzle than for a nozzle array.

After p is eliminated by means of the state equation $p = \rho RT$, the pseudo-one-dimensional flow equations become:

mass conservation equation
$$\frac{\partial \rho}{\partial t} = -u\frac{\partial \rho}{\partial x} - \frac{\rho u}{A}\frac{\partial A}{\partial x} - \rho\frac{\partial u}{\partial x} \tag{25}$$

momentum conservation equation
$$\frac{\partial u}{\partial t} = -u\frac{\partial u}{\partial x} - \frac{RT}{\rho}\frac{\partial \rho}{\partial x} - R\frac{\partial T}{\partial x} \tag{26}$$

energy conservation equation
$$\frac{dE}{dt} = -\frac{uRT}{A}\frac{\partial A}{\partial x} - RT\frac{\partial u}{\partial x} \tag{27}$$

In the above, A = A(x) denotes the cross-section of the nozzle, u is the flow rate and E is the total internal energy of 1 g of gas mixture:

$$E = \frac{5}{2}RT + \frac{X_H}{2}RT + \sum_{i=1}^{3}\frac{N_H k\theta_{Hi}}{e^{\theta_{Hi}/T} - 1} + \sum_{i=1} E_i \tag{28}$$

R is the gas constant for 1 g of gas mixture, X_H is the gram-molecular weight of H_2O, and t=4 denotes the N_2 molecule. 279

If we are only interested in computing small signal gains, then the radiation fields are considered to be approximately zero, and one has

$$\left(\frac{dE_j}{dt}\right)_{\text{radiative}} = \left(\frac{dE_3}{dt}\right)_{\text{radiative}} = 0 \tag{29}$$

Under these conditions, we can write equation (27) as

$$\frac{\partial T}{\partial t} = -u\frac{\partial T}{\partial x} - \frac{1}{\frac{(5+X_H)R}{2} + \sum_{i=1}^{3}\frac{N_H k\theta_{Hi}^2 e^{\theta_{Hi}/T}}{T^2(e^{\theta_{Hi}/T}-1)^2}}\left[\frac{3\theta_2-\theta_3}{3\theta_1}\left(\frac{dE_2}{dt}\right)_{\nu_3\to 3\nu_1} + \left(\frac{dE_2}{dt}\right)_{\nu_2\to T} + \frac{\theta_3-\theta_N}{\theta_1}\left(\frac{dE_3}{dt}\right)_{\nu_3\to\nu_N} + \left(\frac{dE_N}{dt}\right)_{\nu_N\to T} + \frac{uRT}{A}\frac{\partial A}{\partial x} + RT\frac{\partial u}{\partial x}\right] \tag{30}$$

Equations (25), (26), (30) and (9) and the equation (22) obtained after substituting into it equation (29) make up a complete set of equations, with ρ, u, T, E_2, E_3 and E_N as unknown variables.

After the steady-state solutions for the nonequilibrium flow have been found using the non-steady-state method, one needs to further compute for particle number inversion, gain and the maximal useable laser energy. First, we find the vibrational temperatures T_1-T_4. Then, we obtain the density of particles in the upper and lower vibrational energy levels of CO_2, $N^{(V)}_{(001)}$ and $N^{(V)}_{(100)}$, using equations of statistical mechanics.

The gain is [18]

$$G(\nu) = \left(N_2^{(V)} - \frac{g_2}{g_1}N_1^{(V)}\right)\frac{c^2}{8\pi\nu_0^2 t_{sp}}g(\nu)_{\text{radiative}} \tag{31}$$

In the above, $N_2^{(V)}$ and $N_1^{(V)}$ are, respectively, the number of particles per unit volume on the upper and lower vibrational energy levels. g_1 denotes the degree of degeneracy, ν_o is the central frequency of the laser transition, c is the speed of light, $g(\nu)$ is the line shape factor, and t_{sp} is the life of the spontaneous radiation.

From statistical mechanics, the particle number inversion of the p(J) transition of CO_2(001)-(100) is

$$\Delta N^{p(J)} = N_2^{(V)} - \frac{g_2}{g_1} N_1^{(V)}$$
$$= (\alpha N_{001}^{(V)} - N_{100}^{(V)}) \times \frac{2\theta_{r100}(2J+1)}{T} e^{-\theta_{r100} J(J+1)/T} \quad (32)$$

with the factor

$$\alpha = \frac{\theta_{r001} \exp[-\theta_{r001} J(J+1)/T]}{\theta_{r100} \exp[-\theta_{r100}(J+1)(J+2)/T]} \quad (33)$$

The rotational characteristic temperature is determined from spectral constants [19]. The p(20) transition that occurs under most conditions at room temperature is

$$\Delta N^{p(20)} = (\alpha N_{001}^{(V)} - N_{100}^{(V)}) \frac{43.735}{T} \exp(-235.5/T) \quad (34)$$

$$\alpha = 0.992045 \exp(24.12/T) \quad (35)$$

When T is 1500, 1000, 500 and 300°K, α is 1.008, 1.016, 1.041 and 1.075 respectively. Obviously, an error exists in the formula

$$\Delta N_{Anderson}^{p(20)} = (N_{001}^{(V)} - N_{100}^{(V)}) \frac{45.6}{T} \exp(-234/T) \quad (36)$$

that Anderson used to compute gain. When $N_{100}^{(V)} << N_{001}^{(V)}$, the error is 1-8%. The error is even larger when $N_{100}^{(V)}$ is not very much different from $N_{001}^{(V)}$.

Another factor in the gain formula equation (31) that needs to be examined is the line shape factor g(ν). For the CO_2 laser transition, the natural line width is much smaller than the broadening due to collisions and the Doppler effect, and can be neglected. At high cavity pressures, the line width is mainly due to collisions, while at low cavity pressures, it is mainly due to Doppler broadening. For a laser with a typical composition whose cavity is at room temperature, a 1% error will result from considering broadening due to collision only, when the cavity pressure is at 0.1 atm, while a 3% error will result if the same is done when the cavity pressure is 0.05 atm [20]. When only broadening due to collisions is taken into consideration, the formula for calculating the gain near the center

of the spectral line is

$$G^{(J)}(\nu_0) = \Delta N^{(J)} \frac{c^2}{4\pi^2 \nu_0^2 \Delta\nu_\rho} \qquad (37)$$

In the above equation, $\Delta\nu_\rho$ is the half-width of the collision broadening. If one wishes to include the effect of Doppler broadening, a more precise formula may be used [20].

The maximal useable laser energy defined in [7] can be used as a rough estimate of the upper limit of the laser energy extractable from the lasing medium. It is the difference between the vibrational energy stored in CO_2 (ν_3) and $N_2(\nu)$ and the vibrational energy that still remains when the gain has dropped to zero, multiplied by the quantum efficiency. This can be calculated approximately by means of the formula below.

$$E_{max} = \left[E_3(T_3) + E_N(T_N) - E_3\left(\frac{\theta_3}{\theta_1} T\right) - E_N\left(\frac{\theta_3}{\theta_1} T\right)\right] \times 0.409 \qquad (38)$$

IV. Numerical calculations

For the pseudo-one-dimensional nonequilibrium flow equations, we followed the method used in [7], and adopted the difference scheme given in [21]. It is fairly easy to show that this computational scheme possesses second-degree accuracy. The amount of computation is much smaller than that required when a Taylor series expansion with second degree terms is used. The method also lends itself well to computer programming.

A problem that exists in computing for the pseudo-one-dimensional flow using a time-dependent method is that after being brought to the steady state, ρ and u may not necessarily satisfy the condition of mass conservation. Originally, from equation (25), we have

$$\frac{\partial \rho}{\partial t} = -\frac{1}{A} \frac{\partial(\rho u A)}{\partial x} \qquad (39)$$

After the steady state has been reached, $\frac{\partial \rho}{\partial t} = 0$, which means that ρuA is a constant at all points of the nozzle. However, problems inherent in the numerical computation often cause the mass flux of the convergent solution to be different at different positions x.

According to [7], the difference in the values of ρuA at different portions of the nozzle can be as high as 20-30%. We know from equation (39) that

$$\Delta(\rho uA) = |(\rho uA)_{x+\Delta x} - (\rho uA)_x| = \left|\frac{\Delta\rho}{\Delta t}\right| A\Delta x$$

Thus, the difference in the mass fluxes at neighboring mesh points is not only dependent on the difference ratio $\Delta\rho/\Delta t$, but also on the space step size Δx. To reduce the size of $\Delta(\rho uA)$, besides greatly increasing the number of computations so as to absolutely reduce $|\Delta\rho/\Delta t|$, one may resort to the possibly more effective way of increasing the density of the mesh points. Furthermore, substituting the right hand side of equation (39) for the expanded right hand side of equation (25) will also eliminate errors due to computations of the difference ratio, and make $\Delta(\rho uA)$ smaller.

We ran the program that we compiled on the TQ-16 computer made in this country. To examine the various factors that affect the accuracy of computation, and to arrive at a way of reducing computing time under given requirement on accuracy, we first did a large amount of experimentation with numbers.

From 1/3 to 1/2 of the time of computing for each time step is spent on the computation of the relaxation time. The relaxation time is mainly dependent on T which does not vary much between two neighboring time steps, the amount of variation decreasing with increasing convergence. Therefore, we were able to appreciably reduce computing time by means of skipping several time steps before making a computation for the relaxation time τ.

To reduce computing time, Anderson carried out the computation for the entire nozzle in two sections, making use of mesh points with two different space step sizes. We used tri-sectional computation with variable intervals, and carried out the computation in each section only down to a few points downstream the boundary point. This speeded up the computation. However, there is some discrepancy in the results computed for ΔuA at the boundary points from the

281

different sections. These kinks can be smoothed out by means of recalculations using the converged solutions as initial values. Our computations show that such smoothing has but little effect on the gain, E_{max} and flow parameters downstream from the nozzle exit that we are mainly interested in.

Computing time can be significantly reduced by using the converged solutions for a nonequilibrium flow as the initial distribution for another set of solutions for a problem with slightly different conditions. This method is especially useful when one wishes to examine the effects of continual changes in a certain parameter (such as T_0 or p_0, etc.).

We have carefully examined the effects on convergence, accuracy of the results and computing speed of the choice of the position of the boundary point between different sections, the position of the downstream end of each section of computation, the initial value distribution, the density of mesh points in every section of the nozzle, the number of steps one skips before making a calculation of τ, condition for convergence, time step size, and the position of the starting point of the subsonic section of the nozzle (the upstream end of the entire calculation).

It is worth pointing out that when the mesh points are not properly arranged, even though the non-steady-state calculations for the nozzle flow can still converge, there often appears an unsmoothness in the subsonic section. The parameters have fluctuating values instead of values that vary monotonically. These values may even become greater than the stagnation values (such as T, p). Such a phenomenon, which is irrational from the standpoint of physics, is due to improper numerical procedures. This problem can usually be overcome, and a smooth solution can be obtained by increasing the density of mesh points, especially those near the throat. Of course, this lengthens the computing time. Luckily, even if the solution is not smooth, the resulting parameters downstream from the nozzle exit are not much different from those of the smooth solution.

In addition, improper choices of the time step size will also result in an unsmooth, or even divergent, solution.

V. Results and discussion

1. Comparison with experimental results. To examine the effects of improvements made in the relaxation model, the relaxation equations and the data used, as opposed to Anderson's results, we carried out computations for some published experimental results. As the detailed nozzle shape-line data were not supplied in the references, we used in our calculations a nozzle of the smallest length that had the same throat height and approximately the same area ratio. Our calculations show that the small signal gain of the nozzle exit is not sensitive to differences in the shape-lines. (See the results given below).

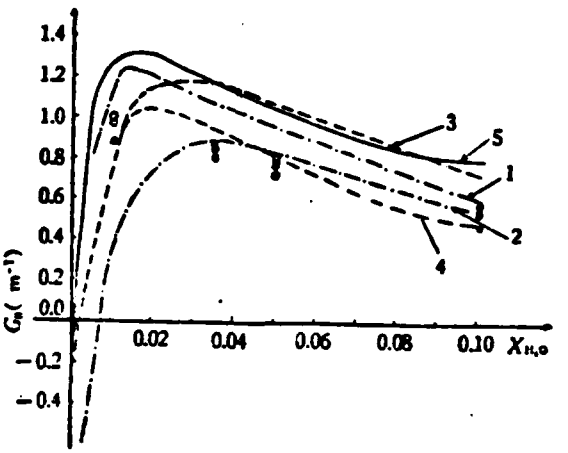

Figure 2. G_0-X_{H_2O} curves (1.27 cm downstream from the nozzle exit)

T_0=1800°K, p_0=37.5 atm, X_{CO_2}=0.07, A_{exit}/A^*=50, h^*=0.0356cm
nozzle of minimum length ⬡ experimental data [14]

1--computed results given in [13], in the absence of Sharma potential barrier; 2--computed results given in [13], in the absence of Sharma potential barrier; 3--computed results given in [7] and [8] (old relaxation rates); 4--computed results given in [17] (new relaxation rates); 5--computed results given in this paper

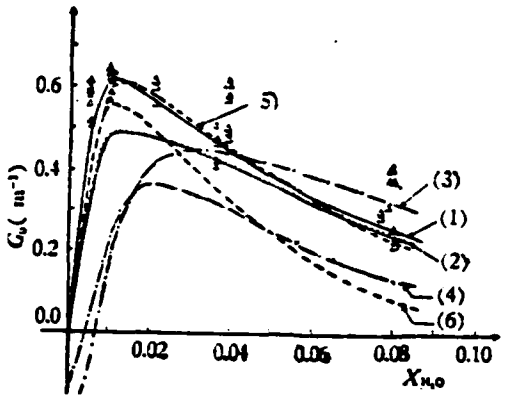

Figure 3. G_0-X_{H_2O} curves (1.27 cm downstream from the nozzle exit) (A comparison of different relaxation models and relaxation rates) T_0=1800°K, p_0=20 atm, X_{CO_2}=0.07, A_{exit}/A^*=20, h*=0.1
nozzle of minimum length Δ experimental data [14]
1--computed results given in this paper; 2--results obtained by using the relaxation rates given in [12] and the relaxation model given in this paper; 3--results obtained by using the relaxation rates given in [7] and [8] (old rates) and the model given in this paper; 4--relaxation rates given by [17] (new rates) and the model given in this paper; 5--relaxation rates given in [7] and [8] (old rates) and Anderson's model (taken from [14]); 6--relaxation rates given in [17] (new rates), and Anderson's model (taken from [14]).

It can be seen from Figures 2 and 3 that Anderson's results do not agree very well with the experimental results for small signal gains. When his new data [17] are used, the results computed for the case with A/A*=50 agree fairly well with experimental results. The results for the nozzle with A/A*=20, however, are much lower than the experimental results. This is inexplicable [14]. In contrast, the tendency of variation of our computed results agree with the experimental data. The theoretical results for the nozzle with A/A*=20 agree with the experimental results, while those for the nozzle with A/A*=50 are higher than the experimental results by about 30%. This is understandable because for a nozzle with greater expansions, the effects of neglecting the non-ideal characteristics of the flow and the two-dimensional effects in the computations, and the nonequilibrium effects of vibration in the design of the nozzle are aggravated. The effects of variations and deviations in the assembly and processing of the nozzles will also be greater (this is almost inevitable). Thus, we may say that our computations have

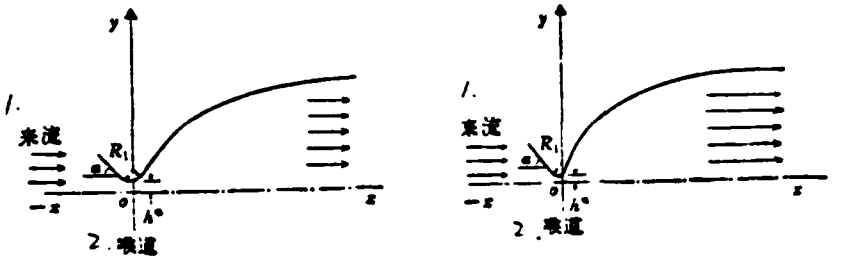

Figure 4. Schematic diagram of the nozzle shape-line (a) nozzle with circular throat; (b) nozzle with minimal length 1--oncoming stream; 2--throat

done away with the inconsistency in Anderson's computations.

It can be seen from Figure 2 that the conclusion that Anderson made from his procedure of computation, which was based on old data and which contained relatively large errors, that increasing the H_2O content of second-generation gasdynamic lasers will keep the gain basically the same is not correct. Actually, the optimal water content of gasdynamic lasers with high area ratios, high stagnation temperatures and high stagnation pressures is still around 1%, the gain decreasing rapidly with increasing water content.

2. Effects of the nozzle shape-line. Supersonic section: We carried out calculations for a nozzle with circular throat and a nozzle with minimal length (Figure 4), with $A/A^* \tilde{\sim} 30$ (M=5.0), under similar conditions. The results are given in Figures 5(a) and 5(b). These show that the gain of the nozzle with minimal length tends to be greater by less than 8% (even less for $T_0 > 1500°K$), and its E_{max} is greater by around 10%. In view of considerations related to processing, assembly and flow fields, it would be all right to give up this advantage and use the nozzle with circular throat instead.

Subsonic section: In the calculations, the subsonic section of the nozzle is made up of a circular arc and a straight line

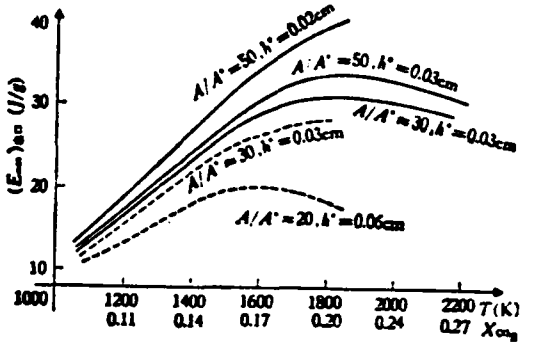

(a) E_{max}-$T(X_{CO_2})$ relation

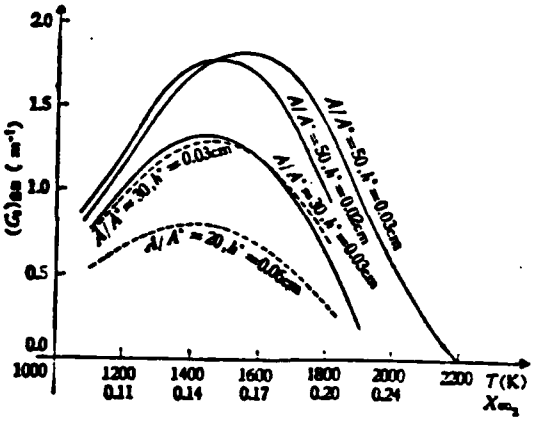

(b) G_0-$T(X_{CO_2})$ relation

Figure 5. Relation between $(E_{max})_{exit}$, $(G_0)_{exit}$ and $T(X_{CO_2})$ (CO gauged combustion) p_o=30 atm, X_{H_2O}=0.01
——nozzle of minimum length ----nozzle with circular throat shape-line

tangent to this arc and at a definite angle with respect to the center line. When the radius R_1 of the arc stays the same while the angle of inclination α varies from 30° to 75°, both G_0 and E_{max} remain basically the same. The G_0 at the nozzle exit varies from 0.796 to 0.799 (m^{-1}), and E_{max} changes from 14.90 to 14.93 (J/g). When the angle of inclination is fixed, G_0 and E_{max} vary with R_1 (Figure 6). It can be seen from Figure 6 that with decreasing radius of the arc of the subsonic section near the throat, both G_0 and E_{max} increase monotonically, and reach their maximum values when the arc becomes a straight line (R_1=0). The range of variation is a few percent. Our computations show that the part of the subsonic section

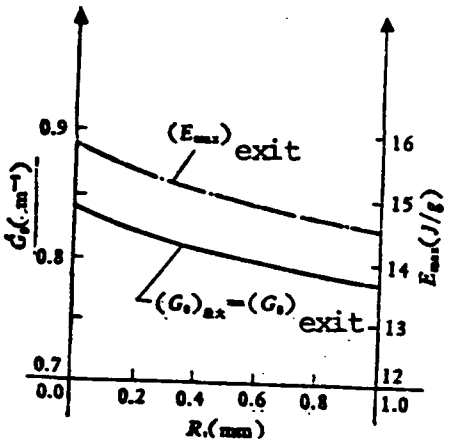

Figure 6. Relation between G_0, E_{max} and R_1. R_1 is the radius of the arc near the throat.

T_o=1300°K p_o=23 atm
A/A*=20 h*=0.06 cm
X_{CO_2}=0.13 X_{N_2}=0.86
α=45° X_{H_2O}=0.01

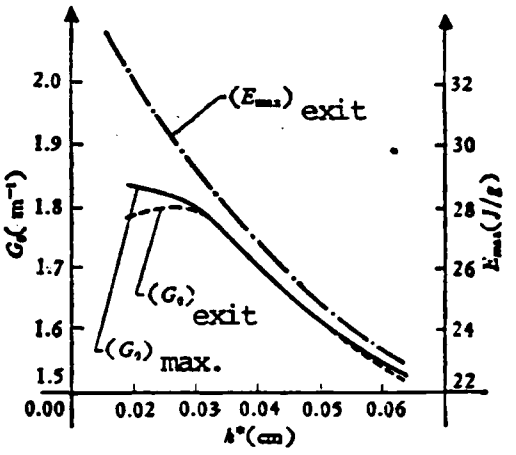

Figure 7. Relation between throat height and G_0, E_{max}

for which the area ratio is greater than 5 there is almost no freezing effect, and its shape-line may be chosen.

Optical cavity section: As the vibrational energy stored in N_2 and CO_2 will eventually be passed to the average motion via relaxation processes, thus raising the temperature of the average motion downstream, this effect will be more pronounced in the presence of laser radiation. To increase the gain downstream, from the optical cavity section, one may allow the optical cavity section to expand further.

3. The effect of the nozzle expansion area ratio. Since the relaxation processes transfer the vibrational energy to the average motion, the temperature of the average motion of the nonequilibrium flow will be higher by several tens of degrees than that computed for an isentropic flow. This is disadvantageous for bringing about population inversion. In order to fully utilize the stored vibrational energy to increase the freezing effect of the nozzle, one may increase the area ratio to reduce the temperature downstream. This

TABLE 2. Relation between stagnation pressure and $G_0(m^{-1})$, $E_{max}(J/g)$

压力 (atm)	$A/A^*\approx 50$, $h^*=0.3$mm, 1500°K, 0.14:0.85:0.01				$A/A^*\approx 30$, $h^*=0.3$mm, 1500°K, 0.14:0.85:0.01			
	出口 G_0	最大 G_0 位置	最大 G_0	出口 E_{max}	出口 G_0	最大 G_0 位置	最大 G_0	出口 E_{max}
23	1.814	下游2cm	1.838	31.26	1.282	下游2cm	1.360	28.54
30	1.799	出口	1.799	29.28	1.286	下游1cm	1.300	26.13
40	1.689	出口	1.689	26.64	1.196	出口	1.196	22.90

1--pressure; 2--G_0 at the exit; 3--location of maximum of G_0; 4--maximum G_0; 5--E_{max} at the exit; 6--downstream; 7--exit

will result in a significant increase in both G_0 and E_{max}, and is a very important means for improving gasdynamic laser performance.

The computed results are given in Figures 5(a) and 5(b). G_0 of the nozzle with A/A*=50 is 30-40% higher than that of the nozzle with A/A*=30, while E_{max} of the former is 5% higher than that of the latter. For combustion type gasdynamic lasers, the optimal value of the stagnation temperature increases slightly with increasing area ratio.

4. Changes in the throat height. Dimensionless mesh parameters are used in nozzle designs. A reduction in the throat height is equivalent to a shortening of the blades. This means that a shorter time is required for reaching the same degree of expansion, which is obviously advantageous for freezing the vibrational energy and bringing about population inversion (Figure 7). Reducing throat height is also one way of improving the performance of the unit. However, reduced throat height and blade length means greater difficulty in blade processing and assembly. In addition, the effect of the boundary layer may become too large to be negligible.

5. Changes in the stagnation temperature. In combustion type gasdynamic lasers, the energy source for the thermal excitation comes

from the combustion of the fuel (e.g., CO_0, H_2). Therefore, changes in the stagnation temperature can be brought about by changes in the composition of the gas mixture. No computation for such conditions with practical significance has been found in the literature. We present our results in Figure 5.

Generally, G_0 has a maximum near 1400-1600°K (the value being slightly different for different shape-lines). E_{max} increases in general with T_0, but the tendency is not very strong at high temperatures. Thus, overly increasing the operating temperature for a given fuel will not be very helpful. Furthermore, higher T_0 means greater heat loss as well as greater difficulty in the manufacture of the unit.

6. Changes in the stagnation pressure. An increase in pressure results in an increase in the density of particles, more frequent collisions and increased relaxation rate. This will cause G_0 and, especially, E_0, to drop. The computational results are as shown in Table 2 and Figure 8. The maxima of E_{max} and G_0 decrease monotonically with increasing p_0, and the optimal point of the gain moves in the upstream direction. All these are disadvantageous for the performance of the unit.

The light output of the operating medium per unit mass can be increased by improving the starting performance of the unit and the performance of the pressure diffuser, and reducing the operating pressure. In contrast, increasing the stagnation pressure will reduce the light output per unit mass, but will increase the totalut output power of a unit of the same size.

7. Changes in the composition. The effect on T_0 of a change in the composition has been given above. In combustion type gasdynamic lasers, inevitable heat losses result in the consumption of more heat than expected to reach the desired T_0, thus causing X_C (or X_H) to increase slightly. To examine this effect, we performed

TABLE 3. Effect of composition on G_0, E_{max}

$X_C:X_N:X_H$	$A/A^*\approx 50$, $h^*=0.3$mm, $p_0=30$atm, $T_0=1500$°K		$A/A^*\approx 30$, $h^*=0.3$mm, $p_0=30$atm, $T_0=1500$°K	
	1. 出口 G_0	2. 出口 E_{max}	1. 出口 G_0	2. 出口 E_{max}
0.14:0.85:0.01	1.799	29.28	1.286	26.13
0.15:0.84:0.01	1.823	28.24	1.297	25.11

1--G_0 at the exit; 2--E_{max} at the exit

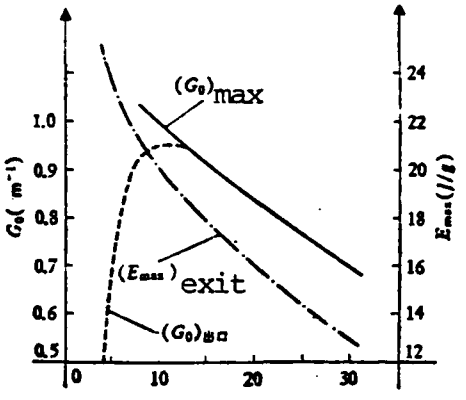

Figure 8. Effect of pressure on G_0, E_{max}
$T_0=1300$°K $A/A^*=18.9$ $h^*=0.06$cm
$X_{CO_2}=0.13$ $X_{H_2O}=0.01$

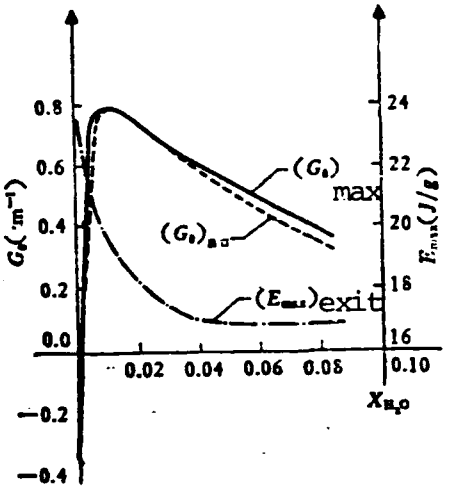

Figure 9. Effect of X_{H_2O} on G_0, E_{max}
$T_0=1500$°K $p_0=23$atm $A/A^*=20$
$h^*=0.06$cm $X_{N_2}=0.85$

the calculations shown in Table 3. It can be seen from this table that G_0 is slightly higher for the gas mixture with a higher composition of the fuel. This is because G_0 is directly proportional to X_C (see Equation (37)). However, an increase in X_C will speed up the release of the vibrational energy, reduce the effective storage of the vibrational energy (X_N decreases), and, therefore, cause E_{max} to drop significantly. Thus, the amount of energy stored in the molecules that can be used for lasing is reduced, and the light output cannot be enhanced. In addition, in the presence of laser radiation, a high X_C has an adverse effect on the saturation effect of the gain. Therefore, in examining the various factors affecting the performance of the unit, one should not just consider the effect on G_0 but should make an overall analysis.

To obtain the same stagnation temperature, one can change the composition of the gas mixture. As the heat of combustion and the specific heat of the products are similar for CO and H_2, one may regard gas mixtures with constant X_C+X_H as having approximately the same stagnation temperature. The results of our computation are given in Figure 9. The optimal water content of combustion type gas-dynamic lasers is also in the neighborhood of 1%. An increase in the water content will cause G_0 and E_{max} to drop sharply. This is because increased water content will greatly increase the radiationless dissipation of vibrational energy.

8. Effects of relaxation model, equations and relaxation data. In [7], [17] and [12], the logarithm of the relaxation time is considered to have a linear relation with $T^{-1/3}$. However, this linear relation does not hold very well in the greater temperature range that includes the lower temperatures. Hence, the use of linear fitting may solve some of the problems while missing out on others. In this paper, we have taken up to the second or third power terms in the relation between the relaxation data and $T^{-1/3}$. Therefore, strictly speaking, our paper is different from the above mentioned papers in the data used for every reaction. We list only the major differences in Table 4. It can be seen from this table that the new rates used in [17] represent changes in the data for two energy exchange reactions only, and the fitting to experimental the relaxation data is still not very good. The results given in [12] are closer to those given in this paper, but there is still a significant difference in the rate of radiationless dissipation of the lower energy level of the laser.

Figure 3 gives the results obtained (curves 1-4) by using our relaxation model and relaxation equations, and several different sets of relaxation data. (As reaction (3) was not taken into consideration in [7], [17] and [12], our data was used for this reaction). It also gives the results taken from [1] which were obtained by using the model and equations as well as the new and old relaxation rates

TABLE 4. A comparison among the relaxation data used in different papers

1. 能量交换反应	τp(μs·atm) \ T(°K) / 2.文献	300	500	1000	1500	1800
$CO_2(\nu_3 \rightarrow 3\nu_2)$-$H_2O$	3.本文	0.045	0.046	0.070	0.093	0.104
	[12]	0.045	0.053	0.073	0.093	0.105
	[7,17]	0.055	0.055	0.055	0.055	0.055
$N_2(\nu = 1 \rightarrow T)$-$H_2O$	3.本文	9.49	3.85	1.83	1.44	1.35
	[12]	8.73	3.79	1.50	1.50	1.50
	[17]	7.75	1.75	0.334	0.151	0.108
	[7]	1052	459.2	182.8	116.6	92.4
$CO_2(\nu_2 \rightarrow T)$-$H_2O$	3.本文	0.00245	0.00697	0.0167	0.0241	0.0231
	[12]	0.00393	0.0118	0.040	0.0725	0.0921
	[7,17]	0.0167	0.0167	0.040	0.0725	0.0921
$CO_2(\nu_2 \rightarrow T)$-$N_2$	3.本文	12.61	4.22	1.25	0.749	0.625
	[12]	11.99	3.010	0.649	0.307	0.227
	[17]	14.19	5.44	1.906	1.17	0.905
	[7]	28.38	10.88	3.810	2.23	1.81
	[8]	2.36	0.91	0.318	0.189	0.151

1--energy exchange reaction; 2--reference; 3--this paper

given in [17] and [7] (curves 5 and 6). Obviously, there exist a large difference between the results obtained by using different sets of relaxation data with the same relaxation model and equations. This point is also borne out by the computation given in [13]. In our opinion, even the new data given in [17] are not adequate enough. A comparison of curves 3 and 5, and curves 4 and 6 shows that a large difference also results from using the same relaxation data but different models and equations. The resulting changes may be very irregular. We may thus deduce that the errors brought about by the relaxation model and equations used in [7] and [17] were for the most part offset by those due to the relaxation data. However, as the cancellation cannot always be complete, one has the irrational phenomena of curve 6 being much lower than the experimental result.

More refined examination and analysis may be made of the effects of relaxation model, relaxation equations and relaxation data on computational results for nonequilibrium flows.

REFERENCES

[1] Anderson, J. D., Jr., AD-A010484(1974). 亦见 Gasdynamic Lasers: An Introduction, Academic Press (1976).

[2] Басов, Н. Г., и др., *ЖТФ*, **38**, 12 (1968), 2031.

[3] Tulip, J. & Seguin, H., *J. Appl. Phys.*, **42**, 9(1971), 3393.

[4] Генералов, Н. А., и др., *ПМТФ*, 5 (1971) 24.

[5] Munjee, S. A., *Phys. Fluids*, **15**, 3(1972), 506.

[6] Brunne, M., et al., *AIAA J.*, **14**, 3(1976), 352.

[7] Anderson, J. D., Jr., *AIAA J.*, **8**, 3(1970), 545; **8**, 12(1970), 2280; AD-718805 (1970); AD-735878(1971).

[8] Anderson, J. D., Jr., et al., *Phys. Fluids*, **13**, 8(1970), 1983.

[9] Anderson, J. D., Jr. & Harris, E. L., *AIAA Paper* 72—143; 亦见 *Laser Focus* (May, 1972), 32.

[10] Lee, G., et al., *AIAA J.*, **10**, 1(1972), 65.

[11] Lee, G., *Phys. Fluids*, **17**, 3(1974), 644.

[12] Brunner, M. J., AD-783213 (1974).

[13] Jones, A. T., *J. Phys. D: Appl. Phys.*, **9**, 8(1976), 1193.

[14] Vamos, J. S., *AIAA Paper* 74—177.

[15] Taylor, R. L. & Bitterman, S., *Rev. Mod. Phys.*, **4**, 1(1969), 26.

[16] MacDonald, J. D., AD-718131(1970).

[17] Anderson, J. D., Jr., *AIAA J.*, **12**, 12(1974), 1690; 亦见 AD-A015790(1974) 或 *AIAA Paper* 74—176.

[18] Yariv, A., Quantum Electronics, Wiley, New York (1957).

[19] Herzberg, G., Infrared and Raman Spectra of Polyatomic Molecules, Van Nostrand, New York (1945).

[20] Penner, S. S., Quantitative Molecular Spectroscopy and Gas Emissivities, Pergamon, London (1959).

[21] MacCormack, R. W., *AIAA Paper* 69—354.

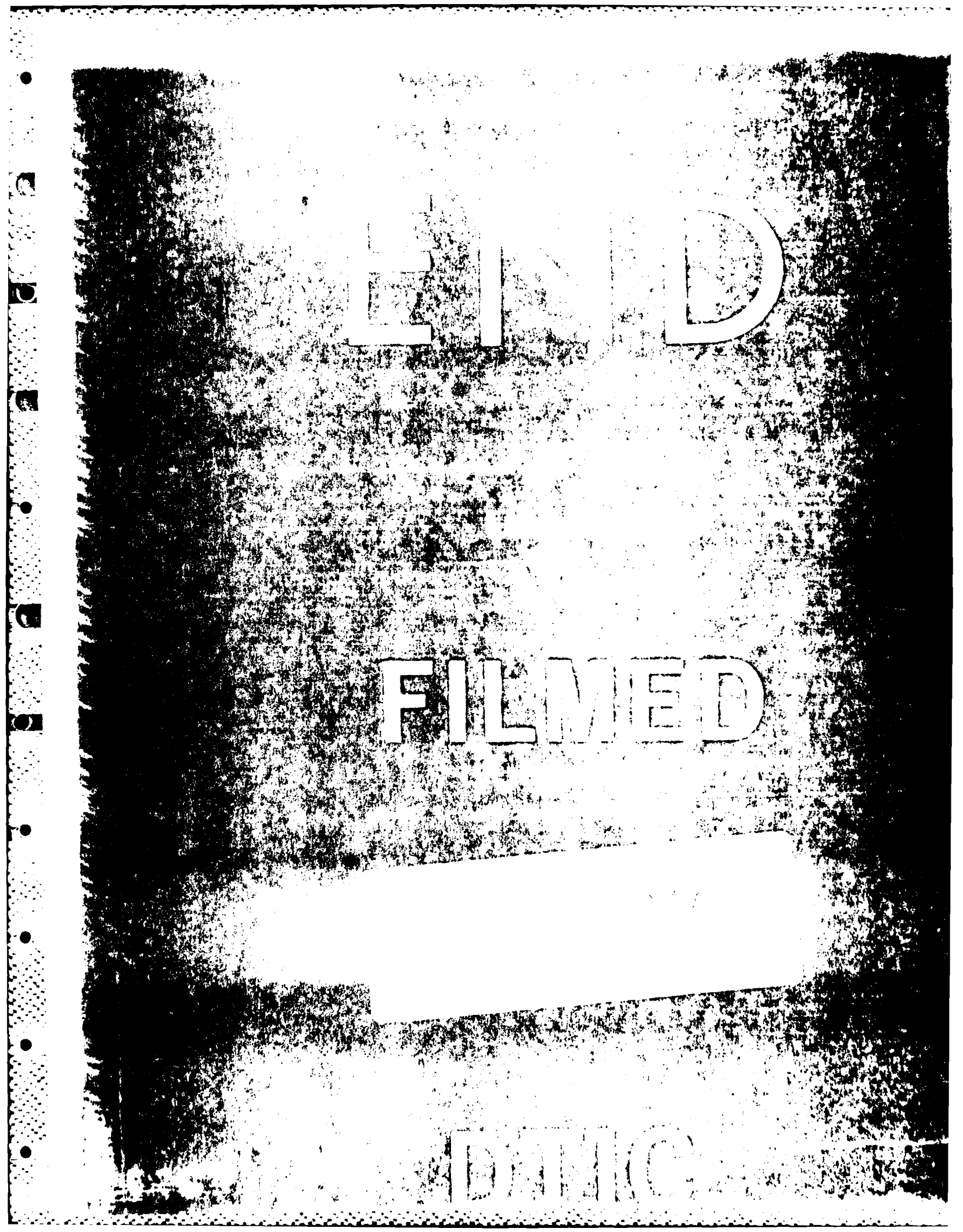
END
FILMED